Speeding Up Proton Transfer in a Fast Enzyme: Kinetic and Crystallographic Studies on the Effect of Hydrophobic Amino Acid Substitutions in the Active Site of Human Carbonic Anhydrase II†

S. Zoë Fisher,‡ Chingkuang Tu,§ Deepa Bhatt,§ Lakshmanan Govindasamy,‡ Mavis Agbandje-McKenna,‡ Robert McKenna,*,‡ and David N. Silverman*,‡,§

Departments of Biochemistry and Molecular Biology, and Pharmacology and Therapeutics, College of Medicine, University of Florida, Gainesville, Florida 32610

Received December 20, 2006

ABSTRACT: Catalysis of the hydration of CO_2 by human carbonic anhydrase isozyme II (HCA II) is sustained at a maximal catalytic turnover of 1 μs^{-1} by proton transfer between a zinc-bound solvent and bulk solution. This mechanism of proton transfer is facilitated via the side chain of His64, which is located 7.5 Å from the zinc, and mediated via intervening water molecules in the active-site cavity. Three hydrophilic residues that have previously been shown to contribute to the stabilization of these intervening waters were replaced with hydrophobic residues (Y7F, N62L, and N67L) to determine their effects on proton transfer. The structures of all three mutants were determined by X-ray crystallography, with crystals equilibrated from pH 6.0 to 10.0. A range of changes were observed in the ordered solvent and the conformation of the side chain of His64. Correlating these structural variants with kinetic studies suggests that the very efficient proton transfer (∼7 μs^{-1}) observed for Y7F HCA II in the dehydration direction, compared with the wild type and other mutants of this study, is due to a combination of three features. First, in this mutant, the side chain of His64 showed an appreciable inward orientation pointing toward the active-site zinc. Second, in the structure of Y7F HCA II, there is an unbranched chain of hydrogen-bonded waters linking the proton donor His64 and acceptor zinc-bound hydroxide. Finally, the difference in pK_a of the donor and acceptor appears favorable for proton transfer. The data suggest roles for residues 7, 62, and 67 in fine-tuning the properties of His64 for optimal proton transfer in catalysis.

The phenomenon of long-range proton transfer has been observed in many biological systems, including bacteriorhodopsin, cytochrome *c* oxidase, adenosine 5′-triphosphate synthase, and the photosynthetic reaction center. Catalysis by human carbonic anhydrase isozyme II (HCA II),[1] one of the fastest enzymes known, is sustained at a maximal catalytic turnover near 1 μs^{-1} in the hydration of CO_2. HCA II is a simple model system for studying long-range proton transfer in a protein, because the rate-limiting step in the maximal velocity of catalysis is the transfer of a proton through intervening solvent molecules between the catalytic zinc-bound solvent and a proton shuttling residue His64, which is located ∼7.5 Å from the zinc (*1*). It has been suggested that efficient shuttling may require some conformational mobility of the side chain of His64 (*2*). Crystal structures of HCA II show about equal occupancy of inward (directed toward the active site) and outward (directed away from the active site) conformations of the side chain of His64 (*3*, *4*). The structure of the active site of HCA II has been well-characterized, and several amino acids (Tyr7, Asn62, His64, Asn67, Thr199, and Thr200) appear to be involved in the stabilization of a network of ordered water molecules observed in crystal structures (Figure 1; $Zn-H_2O/OH^-$, W1, W2, W3a, and W3b), which offer strong clues as to the pathway of the intramolecular proton transfer between the zinc-bound solvent and His64 (*3*−*5*).

HCA II catalyzes the hydration/dehydration of CO_2 in two separate and distinct steps, eqs 1 and 2 (*5*−*7*).

$$CO_2 + EZnOH^- \rightleftharpoons EZnHCO_3^- \overset{H_2O}{\rightleftharpoons} EZnH_2O + HCO_3^- \quad (1)$$

$$His64-EZnH_2O + B \rightleftharpoons H^+His64-EZnOH^- + B \rightleftharpoons His64-EZnH_2O + BH^+ \quad (2)$$

Here, B is an exogenous proton acceptor from solution. The rate-determining step in the maximal velocity of catalysis by HCA II is the proton transfer of eq 2, in which a solvent-accessible His64 in the active-site cavity acts as the proton shuttle in the catalysis (*1*, *8*). Replacement of His64 with Ala (H64A HCA II) results in a 10−50-fold decrease in the

† This work was funded by grants from the National Institutes of Health (Gm25154) and the Thomas Maren Foundation.

* To whom correspondence should be addressed: Box 100267 Health Center, University of Florida, Gainesville, FL 32610-0267. Telephone: (352) 392-3556. Fax: (352) 392-9696. E-mail: silvermn@college.med.ufl.edu (D.N.S.); Box 100245 Health Center, University of Florida, Gainesville, FL 32610-0245. Telephone: (352) 392-5696. E-mail: rmckenna@ufl.edu (R.M.).

‡ Department of Biochemistry and Molecular Biology.

§ Department of Pharmacology and Therapeutics.

[1] Abbreviations: HCA II, human carbonic anhydrase isozyme II; SHIE, solvent hydrogen isotope effect; 4-MI, 4-methylimidazole; PDB, Protein Data Base.

10.1021/bi602620k CCC: $37.00 © 2007 American Chemical Society
Published on Web 03/02/2007

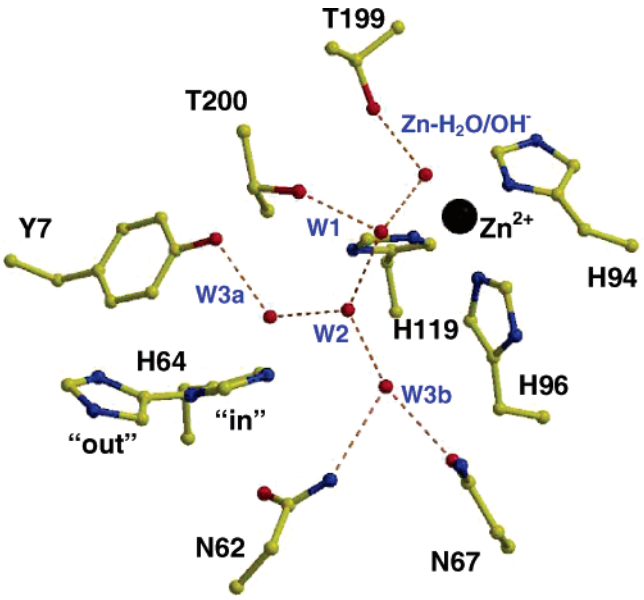

FIGURE 1: Crystal structure of the active site of wild-type HCA II at pH 7.0. Red spheres represent ordered water molecules and are numbered (W1, W2, W3a, and W3b), and red dashed lines indicate distances consistent with hydrogen bonds (2.6−3.2 Å). The side chain of His64 is shown in the inward and outward conformations. Data are from Fisher et al. (*4*).

rate of catalysis compared with the wild type (*1*, *9*). Previous studies have focused on the relation of the active-site water structure with catalysis. Jackman et al. (*10*) replaced Ala65 in HCA II with a series of amino acids to determine that disruption of the ordered solvent network observed in the crystal structure was related to a decrease in proton transfer in catalysis.

We have perturbed the structure of ordered water in HCA II by replacing three hydrophilic residues within the active-site cavity with hydrophobic residues (Y7F, N62L, and N67L), and the effects of these substituents on proton transfer in the catalysis were measured. The X-ray crystal structure of HCA II shows that each of these side chains (Tyr7, Asn62, and Asn67) are hydrogen-bonded to ordered water molecules in the active-site cavity (Figure 1) (*3*, *4*). The X-ray crystal structures of the corresponding three site-specific mutants at 1.8−1.15 Å resolution show a range of side-chain orientations for His64 and a number of changes in the ordered water structure. The data suggest that the very efficient proton transfer (~7 μs^{-1}) observed for Y7F HCA II compared with that of the wild type (~1 μs^{-1}) and the other mutants of this study is due to several features of the structure that we have observed. First, in this mutant, the side chain of His64 showed an appreciable inward orientation pointing toward the active-site zinc. Second, in the structure of Y7F HCA II, there is observed a nearly linear array of hydrogen-bonded water molecules, not branched, between the proton donor His64 and acceptor zinc-bound hydroxide. Finally, the pK_a of the imidazole ring of His64 is more acidic and hence a better proton donor in Y7F HCA II. These features of residue 7 as well as related results for residues 62 and 67 demonstrate a function in fine-tuning the proton-transfer properties of His64.

MATERIALS AND METHODS

Enzyme Preparation. Mutants of HCA II were made by site-directed mutagenesis using expression vectors containing the HCA II coding region (*1*, *11*). Residue Tyr7 was mutated to Phe, and residues Asn62 and Asn67 were separately mutated to Leu using a plasmid encoding the sequence of wild-type HCA II. Plasmids with the appropriate mutations in the cDNA of HCA II were made by site-directed mutagenesis using the Qiagen QuikChange II kit. The sequences of these mutants were confirmed by sequencing the DNA of the entire coding region for CA in the expression vector. Expression of the mutated vectors was done by transforming into *Escherichia coli* BL21(DE3)pLysS, which does not express any indigenous CA under our conditions. Purification of these mutants was performed by using affinity chromatography on a gel containing *p*-(aminomethyl)-benzene-sulfonamide coupled to agarose beads (*12*), followed by dialysis against a 15 mM Tris solution at pH 8.0. HCA II and these mutants bind sulfonamides tightly; therefore, the enzyme concentration was determined by titration of active sites with ethoxzolamide measured by the ^{18}O exchange between CO_2 and water, analyzing data with the Henderson approach (*13*). Concentrations determined in this manner were in agreement with those determined from the molar absorptivity at 280 nm of wild-type HCA II (5.5×10^4 M^{-1} cm^{-1}). Electrophoresis on a 10% polyacrylamide gel stained with Coomassie Blue was used to confirm that the purity of the enzyme samples was greater than 98%.

Oxygen-18 Exchange. This method is based on the depletion of ^{18}O from species of CO_2 as measured by membrane inlet mass spectrometry (*14*). CO_2 passing across the membrane enters a mass spectrometer (Extrel EXM-200) providing a continuous measure of isotopic content of CO_2. In the first stage of catalysis, the dehydration of labeled bicarbonate has a probability of transiently labeling the active site with ^{18}O (eq 3). In a subsequent step, the protonation of the zinc-bound ^{18}O-labeled hydroxide results in the release of $H_2{}^{18}O$ to the solvent (eq 4).

$$HCOO^{18}O^- + EZnH_2O \rightleftharpoons EZnHCOO^{18}O^- \rightleftharpoons COO + EZn^{18}OH^- \quad (3)$$

$$H^+His64{-}EZn^{18}OH^- \rightleftharpoons His64{-}EZnH_2{}^{18}O \overset{H_2O}{\rightleftharpoons} His64{-}EZnH_2O + H_2{}^{18}O \quad (4)$$

This ^{18}O-exchange approach yields two rates for the ^{18}O exchange catalyzed by carbonic anhydrase (*14*). The first is R_1 the rate of exchange of CO_2 and HCO_3^- at chemical equilibrium (eq 3), as shown in eq 5

$$R_1/[E] = k_{cat}^{ex}[S]/(K_{eff}^{S} + [S]) \quad (5)$$

Here, k_{cat}^{ex} is a rate constant for maximal interconversion of the substrate and product, K_{eff}^{S} is an apparent binding constant for the substrate to enzyme, and [S] is the concentration of the substrate, either CO_2 or bicarbonate (*15*). The ratio k_{cat}^{ex}/K_{eff}^{S} is, in theory and in practice, equal to k_{cat}/K_m obtained by steady-state methods.

A second rate determined by the ^{18}O-exchange method is R_{H_2O}, the rate of release from the enzyme of water bearing substrate oxygen (eq 4). This is the component of the ^{18}O exchange that is dependent upon the donation of protons to the ^{18}O-labeled zinc-bound hydroxide (*1*, *14*). In such a step, His64 as a predominant proton donor in the catalysis provides a proton (eq 4). The value of R_{H_2O} can be interpreted in terms of the rate constant for proton transfer from His64 to the zinc-bound hydroxide according eq 6, in which k_B is the rate constant for proton transfer to the zinc-bound hydroxide and $(K_a)_{donor}$ and $(K_a)_{ZnH_2O}$ are the ionization constants of the proton donor and zinc-bound water molecule. The determination of the kinetic constant k_B and ionization constants of eq 6 was carried out by nonlinear least-squares methods (Enzfitter, Elsevier-Biosoft, Cambridge, U.K.).

$$k_B^{obs} = k_B/\{[1 + (K_a)_{donor}/[H^+]][1 + [H^+]/(K_a)_{ZnH_2O}]\} \quad (6)$$

The uncatalyzed and carbonic-anhydrase-catalyzed exchanges of ^{18}O between CO_2 and water at chemical equilibrium were measured in the absence of buffer unless stated otherwise at a total substrate concentration of 25 mM, using membrane-inlet mass spectrometry (*14*). The temperature was 25 °C, and the total ionic strength of the solution was kept at a minimum of 0.2 M by the addition of Na_2SO_4.

Stopped-Flow Spectrophotometry. Initial rates of CO_2 hydration were measured by following the change in absorbance of a pH indicator on an Applied Photophysics (SX.18MV) stopped-flow spectrophotometer (*16*). The pK_a values and wavelengths for the pH indicator−buffer pairs used to create pH profiles were as follows: 2-(*N*-morpholino)ethanesulfonic acid (MES) (pK_a = 6.1) and chlorophenol red (pK_a = 6.3), λ = 574 nm; 3-(*N*-morpholino)propanesulfonic acid (MOPS) (pK_a = 7.2) and *p*-nitro phenol (pK_a = 7.1), λ = 401 nm; *N*-2-hydroxyethylpiperazine-*N*′-2-ethanesulfonic acid (HEPES) (pK_a = 7.5) and phenol red (pK_a = 7.5), λ = 557 nm; tris-aminopropanesulfonic acid (TAPS) (pK_a = 8.4) and *m*-cresol purple (pK_a = 8.3), λ = 578 nm; and 2-(cyclohexylamino)ethylsulfonic acid (CHES) (pK_a = 9.3) and thymol blue (pK_a = 8.9), λ = 596 nm. Final buffer concentrations were 25 mM, and the total ionic strength was kept at 0.2 M by the addition of Na_2SO_4. CO_2 solutions were prepared by bubbling CO_2 into water at 25 °C with final concentrations after mixing ranging from 0.7 to 17 mM. The mean initial rates at each pH were determined from 5 to 8 reaction traces comprising the initial 10% of the reaction. The uncatalyzed rates were determined in a similar manner and subtracted from the total observed rates. Determination of the kinetic constants k_{cat} and k_{cat}/K_m were carried out by a nonlinear least-squares method (Enzfitter, Elsevier-Biosoft).

Esterase Activity. The catalysis by HCA II and mutants of the hydrolysis of 4-nitrophenylacetate was measured by the method of Verpoorte et al. (*17*), in which the increase in absorbance was followed at 348 nm, the isosbestic point of nitrophenol and the conjugate nitrophenylate ion using the molar absorbtivity 5.0×10^3 M^{-1} cm^{-1}. A Beckman Coulter DU 800 spectrophotometer was used to measure initial velocities. The buffers used at 25 mM were as identified in the previous paragraph. The rate constants k_{enz} reported here represent k_{cat}/K_m for the catalyzed hydrolysis. The value of K_m is too large to measure k_{cat}.

Solvent Hydrogen Isotope Effects (SHIEs). We measured SHIEs; that is, the ratio of rate constants in H_2O to that in 99% D_2O. Deuterium oxide (99.9% D_2O) was obtained from Sigma-Aldrich and distilled from activated charcoal before use. Measurements of pH in these experiments are uncorrected pH-meter readings, done to allow partial cancellation of two factors: the correction required of a pH-meter to account for solvent D_2O and the changes in pK_a for almost all acids in the region of pK_a from 3 to 10 (*18*).

Crystallography. Crystals of the HCA II single-site mutants were obtained using the hanging-drop vapor-diffusion method (*19*). The crystallization drops were prepared by mixing 5 μL of protein [concentration of ∼10 mg/mL in 50 mM Tris-HCl (pH 7.8)] with 5 μL of the precipitant solution [50 mM Tris-HCl (pH 8.2) and 2.6 M ammonium sulfate] at 293 K against 1000 μL of the precipitant solution. Useful crystals were observed 2 days after the crystallization setup. The different pH values (pH 6.0, 8.2, and 10.0) of the crystals were obtained by equilibrating crystals in appropriate buffers [50 mM MES at pH 6.0, 50 mM Tris at pH 8.2, and 50 mM 3-(cyclohexylamino)-1-propanesulfonic acid (CAPS) at pH 10.0] and 2.6 M ammonium sulfate. Crystals of Y7F HCA II at pH 9.0 were obtained with 1.2 M sodium citrate as the precipitant [100 mM Tris-HCl (pH 9.0)] using the same methods as described above. The pH stated is that measured at the start of the experiment.

The X-ray diffraction datasets for all of the mutant HCA II crystals (except the Y7F HCA II at pH 9.0 data) were obtained at room temperature, using an R-AXIS IV++ image plate system with Osmic mirrors and a Rigaku HU-H3R Cu rotating anode operating at 50 kV and 100 mA. The detector−crystal distance was set to 100 mm. Each dataset was collected at room temperature from one to three crystals mounted in quartz capillaries. The oscillation steps were 1° with a 7 min exposure per image. X-ray data processing was performed using DENZO and scaled and reduced with SCALEPACK (*20*). Dataset statistics for N62L and N67L HCA II are given in Table 1a.

The X-ray diffraction dataset for the Y7F-HCA II (pH 9.0) crystal from the sodium citrate condition was collected at the Advanced Photon Source (APS) beamline SER-CAT-22-ID with a wavelength of 0.9793 Å. The crystal was quick-dipped in a cryo-protectant (20% glycerol in precipitant solution) prior to flash cooling and data collection at 100 K. The crystal−detector distance was 100 mm, and 260° of data with 1 s exposures were recorded to 1.15 Å resolution on a CCD detector. All data were indexed, scaled, and reduced with HKL2000 (*20*). All Y7F HCA II dataset statistics are given in Table 1b.

All manual model building was performed using Coot (*21*), and refinement was carried out with the crystallography and nuclear magnetic resonance (NMR) system (CNS) suite of programs, version 1.1 (*22*). The wild-type HCA II crystal space group [Protein Data Bank (PDB) accession code 1TBT (*4*)] and therefore was isomorphous with all of the datasets collected, was used to phase the datasets. To avoid phase bias of the model, the zinc ion, mutated residues, and water

Table 1: Dataset, Refinement, and Final Model Statistics for the Crystallographic Study of (a) N62L and N67L HCA II and (b) Y7F HCA II

(a)	N62L at pH 8.2[a]	N67L at pH 8.2[a]	N62L at pH 6.0[a]	N67L at pH 6.0[a]
unit cell dimensions [a, b, c (Å), β **(deg)]**	42.8, 41.7, 72.9, 104.8	42.6, 41.7, 73.0, 104.6	42.8, 41.6, 73.0, 104.7	42.6, 41.6, 73.0, 104.5
resolution (Å)	20.0−1.70	20.0−1.65	20.0−1.80	20.0−1.80
number of unique reflections	25 698 (2422)	27 340 (2590)	20 541 (2031)	21 266 (2142)
completeness (%)	93.1 (88.9)	91.0 (87.4)	88.2 (86.9)	91.7 (92.6)
redundancy	3.2 (3.3)	3.1 (3.1)	4.1 (4.0)	3.4 (3.2)
R_{symm}[b]	0.108 (0.286)	0.085 (0.448)	0.106 (0.339)	0.075 (0.349)
number of protein/solvent atoms	2058/132	2058/116	2058/108	2058/97
R_{cryst}[c]/R_{free}[d]	0.179/0.217	0.186/0.201	0.189/0.226	0.187/0.224
average B factor (Å^2)				
main/side chain	16.1/19.5	18.2/21.4	16.8/20.1	18.6/22.2
Zn/solvent/sulfate	10.4/29.6/na	11.5/29.6/na	10.5/28.7/29.7	13.4/29.5/31.8

(b)	Y7F at pH 8.2[a]	Y7F at pH 10.0[a]	Y7F at pH 9.0[a]
unit cell dimensions [a, b, c (Å), β **(deg)]**	42.8, 41.7, 72.9, 104.7	42.9, 41.7, 73.0, 104.8	42.3, 41.4, 72.3, 104.3
resolution (Å)	20.0−1.70	20.0−1.80	20.0−1.15
number of unique reflections	25 613 (2444)	20 874 (1951)	85 073 (8284)
completeness (%)	92.7 (89.8)	89.4 (83.9)	99.1 (96.8)
redundancy	3.9 (3.9)	3.1 (3.2)	4.2 (3.2)
R_{symm}[b]	0.060 (0.332)	0.071 (0.238)	0.079 (0.364)
number of protein/solvent atoms	2057/115	2057/115	2057/270
R_{cryst}[c]/R_{free}[d]	0.181/0.199	0.179/0.200	0.161/0.186
average B factor (Å^2)			
main/side chain	16.6/20.1	15.1/18.5	11.3/16.1
Zn/solvent/sulfate	10.4/29.4/33.4	10.0/28.3/29.4	7.3/27.1/na

[a] Values in parentheses are for the highest resolution shell. [b] $R_{symm} = \sum|I - \langle I\rangle|/\sum\langle I\rangle$. [c] $R_{cryst} = \sum||F_o| - |F_c||/\sum|F_o|$. [d] R_{free} is calculated the same as R_{cryst} for data omitted from refinement (5% of reflections for all datasets).

molecules were removed. After one cycle of rigid-body refinement, annealing by heating to 3000 K with gradual cooling, geometry-restrained position refinement, and temperature-factor refinement, $2F_o - F_c$ and $F_o - F_c$ Fourier electron-density maps were generated. These electron-density maps clearly showed the position of the zinc and mutated residues, which were subsequently built into their respective models. After several cycles of refinement, solvent molecules were incorporated into the models using the automatic water-picking program in CNS until no more water molecules were found at a 2.0σ level. Refinement of the models continued until convergence of R_{cryst} and R_{free} was reached.

The refinement of the Y7F HCA II (pH 9.0) structure, which diffracted to 1.15 Å resolution, was continued further using SHELXL97 with the conjugate-gradient least-squares (CGLS) mode using default restraints for protein geometry (*23*, *24*). After each round of CGLS refinement, $F_o - F_c$ and $2F_o - F_c$ electron-density maps were generated and the model and maps were visually inspected using Coot (*21*). All non-hydrogen atoms were refined anisotropically using SHELXL97 default anisotropic displacement parameters. Refinement of all models continued until convergence of R_{cryst} and R_{free} was reached.

All refinement and final model statistics are given in parts a and b of Table 1.

RESULTS

The site-specific mutants Y7F, N62L, and N67L HCA II were investigated for their catalytic properties, both in the interconversion of CO_2 and bicarbonate (eqs 1 and 3) and in the proton-transfer-dependent components of catalysis (eqs 2 and 4). In addition, the crystal structures of these variants of HCA II were determined.

Catalyzed Exchange of ^{18}O. The pH dependence of the constant k_{cat}^{ex}/K_{eff}^{S} for the hydration of CO_2 was determined for each mutant from ^{18}O exchange using mass spectrometry (eqs 3 and 5). The pH profiles for k_{cat}^{ex}/K_{eff}^{S} were quite similar over the pH range from 5 to 9 (Figure 2). The values of the kinetic $pK_{a\ ZnH_2O}$ from these data represent the ionization of the zinc-bound water (*8*, *15*). The apparent values of $pK_{a\ ZnH_2O}$ were in the range from 6.4 to 7.3 determined from these pH profiles (Table 2). Maximal values of k_{cat}^{ex}/K_{eff}^{S} from 90 to 140 $\mu M^{-1}\ s^{-1}$ were determined for these variants of HCA II (Table 3). These are similar to values for wild-type HCA II also given in these tables determined in this and prior studies (*6*, *8*, *16*).

The rate constants R_{H_2O}/[E] measured by ^{18}O exchange are determined by the transfer of protons between the zinc-bound solvent molecule and His64 in wild-type HCA II (*1*, *8*). The rate constant R_{H_2O}/[E] measures the proton-transfer-dependent release of $H_2{}^{18}O$ from the enzyme (eq 4) and is determined at chemical equilibrium, which has the advantage that measurements can be made in the absence of buffers, because pH control is not a significant problem. Buffers can participate in proton transfer and complicate interpretation. The pH profiles for the rate constant R_{H_2O}/[E] are complex but appear bell-shaped for much of the region between pH 6 and 9 (Figure 3). The bell-shaped components of R_{H_2O}/[E] were fit to eq 6 describing the proton transfer in terms of the ionization constants of His64 and the zinc-bound water molecule, an equation that has been used previously to

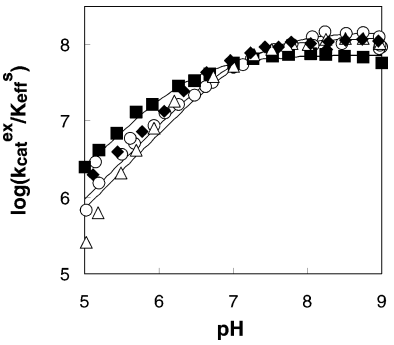

FIGURE 2: pH profiles for k_{cat}^{ex}/K_{eff}^{S} for the hydration of CO_2 catalyzed by the following variants of HCA II: (◆) wild type, (△) Y7F, (○) N62L, and (■) N67L. Data were obtained by ^{18}O exchange using solutions at 25 °C containing 25 mM of all species of CO_2 at sufficient Na_2SO_4 to maintain 0.2 M ionic strength. No buffers were added.

Table 2: Apparent Values of pK_a Obtained by Various Kinetic Measurements of Catalysis by HCA II and Mutants

enzyme	p$K_{a\ His64}$[a]	p$K_{a\ ZnH_2O}$[a]	p$K_{a\ ZnH_2O}$[b] (k_{cat}^{ex}/K_{eff}^{S})	p$K_{a\ ZnH_2O}$ (esterase)
wild type	7.2	6.8	6.9	6.9
Y7F	6.0[c]	7.0[c]	7.1[c]	7.0
N67L	7.5	6.0	6.4	6.7
N62L	*d*	*d*	7.3	7.0

[a] Measured from the fits of eq 6 to the data of Figure 3. The values of the p$K_{a\ ZnH_2O}$ have a standard errors generally near ±0.1 and no greater than ±0.2. [b] Measured from the data of Figure 2. As evident in Figure 2, small perturbations were observed that could be fit by including a second ionization; however, these were not included in this table. The standard errors in pK_a are mostly ±0.1 and no greater than ±0.2. [c] These measurements were at 10 °C to enhance stability; the plot is shown in Figure 4. All other data in the table were obtained at 25 °C. [d] The pH profile was irregular, with no predominant ionizations apparent (Figure 3).

describe this process (*11*, *25*). This procedure gave an excellent fit to the experimental values of R_{H_2O}/[E] for the wild type and N67L HCA II, as shown by the solid lines in Figure 3, with parameters for the constants of eq 6 measured at 25 °C given in Table 3. The fit of eq 6 to the data for Y7F HCA II was not adequate because of instability at low pH; we measured this pH profile at 10 °C, data for which are adequately represented by eq 6 (Figure 4). The pH profile for N62L HCA II showed only a complex pH dependence at pH 5−7 (Figure 3), making interpretation difficult.

The fit of the data for R_{H_2O}/[E] using eq 6 gives estimates of the pK_a for the donor (His64) and acceptor (zinc-bound water) (Table 2), as well as a rate constant for proton-transfer k_B in the dehydration direction (Table 3). The data demonstrate that the values of p$K_{a\ ZnH_2O}$ of the zinc-bound water near 7 for the wild type and Y7F and to a lesser extent N67L HCA II are confirmed by independent measurements of p$K_{a\ ZnH_2O}$ from k_{cat}^{ex}/K_{eff}^{S} for hydration and k_{cat}/K_m for catalysis of the hydrolysis of 4-nitrophenylacetate (Table 2). These assignments of pK_a values are used to determine values of k_B from fits of eq 6. These fits also allow an estimate of the pK_a of His64, which is shown in Table 2; note that this pK_a at 6.0 for Y7F is lower than that for wild-type HCA II.

With appropriate assignments of pK_a, values of k_B could be determined. The values of k_B varied considerably from about 4 μs^{-1} for Y7F HCA II (measured at 10 °C; a value of 7 μs^{-1} is estimated at 25 °C), which was considerably greater than the value 0.8 μs^{-1} for the wild type, to 0.2 μs^{-1} for N67L HCA II. The SHIE on k_B for catalysis by Y7F HCA II was 2.5 ± 0.3, measured at an uncorrected pH-meter reading of 6.2, at the maximum of the pH profile. This value is consistent with rate-limiting proton transfer.

The varied access of buffers to the active site is demonstrated by the activation of R_{H_2O}/[E] by added 4-methylimidazole (4-MI, pK_a = 7.8), shown in Figure 5. Here, clearly, 4-MI is a more efficient activator for Y7F HCA II than the other variants likely because of enhanced access to the active site. The downward slope observed for wild-type and Y7F HCA II at higher concentrations of 4-MI is due to an inhibition at higher concentrations of 4-MI. This effect was studied by Elder et al. (*26*).

Stopped-Flow Spectrophotometry. Values of k_{cat}/K_m for hydration predominantly depend upon the fraction of the aqueous ligand of the zinc that occurs in the zinc-bound hydroxide form (*8*). Maximal values of k_{cat}/K_m for hydration are given in Table 3 for the enzymes of this study. The SHIE on k_{cat}/K_m for dehydration by Y7F HCA II (uncorrected pH-meter reading 5.6) was 0.74 ± 0.07. Values of the steady-state constant k_{cat} for hydration have a maximum at high pH (*8*). The pH profiles for the steady-state constant k_{cat} for the hydration of CO_2 catalyzed by variants of HCA II had considerable scatter, with individual points clustered or grouped according to the buffer used (Supplementary Figure 1 in the Supporting Information). This feature is due, in part, to varied access of buffers as proton acceptors in the active-site cavity. Nevertheless, the data do show the expected increase in k_{cat} with increasing pH; maximal values of k_{cat} are given in Table 3. The SHIE on k_{cat} for dehydration by Y7F HCA II (uncorrected pH-meter reading 5.6) was 0.81 ± 0.10.

Esterase Activity. As another measure of catalysis and the ionization of the zinc-bound water molecule, we determined the capacity of the mutants of Table 2 to catalyze the hydrolysis of 4-nitrophenyl-acetate (*17*). In this case, we measured the pH profile of k_{cat}/K_m for hydrolysis; K_m is too large to allow for the measurement of k_{cat} for this esterase function. The data were fit to a single ionization (Supplementary Figure 2 in the Supporting Information), with values of the kinetic pK_a between 6.7 and 7.0 (Table 2), a measure of the ionization of the zinc-bound water. The maximal value of k_{cat}/K_m for Y7F in this esterase function was significantly larger and the maximal value of k_{cat}/K_m for N67L was significantly smaller than that of the wild type (Table 3).

Crystallography. All crystals were isomorphous and belonged to space group $P2_1$ with mean unit cell dimensions: a = 42.7 ± 0.3 Å, b = 41.6 ± 0.2 Å, c = 72.9 ± 0.5 Å, and β = 104.6 ± 0.3°. The HCA II mutant datasets collected at pH 8.2 were processed to 1.70−1.65 Å resolution, while the other pH datasets were processed to 1.8 Å resolution. In addition, the structure of Y7F HCA II at pH 9.0 was collected at APS and processed to 1.15 Å resolution. A summary of the datasets and final model statistics are given in parts a and b of Table 1.

Atomic coordinates for Y7F [pH 8.2 and 10.0 (ammonium sulfate) and pH 9.0 (sodium citrate)], N62L [pH 8.2 and 6.0 (ammonium sulfate)], and N67L [pH 8.2 and 6.0 (ammonium sulfate)] HCA II have been deposited with the PDB as entries 2NXR, 2NXS, and 2NXT; 2NWO and 2NWP; and 2NWY and 2NWZ, respectively.

Table 3: Maximal Values of Rate Constants for the Hydration of CO_2, Dehydration of Bicarbonate, and Hydrolysis of *p*-Nitrophenylacetate Catalyzed by HCA II and Variants[a]

variant of HCA II	orientation of His64	$(k_{cat}^{ex}/K_{eff}^{S})^b$ hydration (μM^{-1} s^{-1})	$(k_{cat}/K_m)^c$ hydration (μM^{-1} s^{-1})	k_{cat}/K_m esterase (M^{-1} s^{-1})	k_{cat}^c hydration (μs^{-1})	k_B^b dehydration (μs^{-1})	k_{cat}^c dehydration (μs^{-1})
wild type	in/out	120	120	2800	1.4	0.8	0.29
Y7F	in	120	100	4400	1.4	3.9[d]	0.05
N67L	out	90	80	1150	1.0	0.2	0.05
N62L	in	140	100	2050	0.4	0.1[e]	0.10

[a] The standard errors for these rate constants are generally 20% or less. [b] Measured from the exchange of ^{18}O between CO_2 and water using eqs 5 and 6. [c] Measured by stopped-flow spectrophotometry. [d] These measurements were at 10 °C to enhance stability; the plot is shown in Figure 4. All other data were obtained at 25 °C. [e] The pH profile was irregular, with no predominant ionizations apparent (Figure 3). We estimate k_B as the maximal value of R_{H_2O}/[E] from Figure 3.

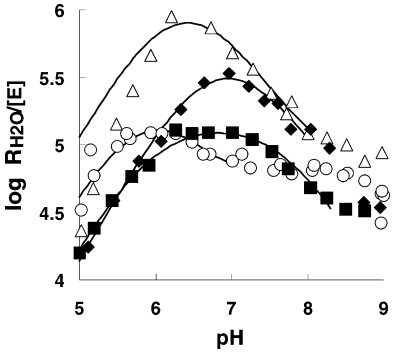

FIGURE 3: pH profiles for R_{H_2O}/[E], the rate constant for the release of $H_2{}^{18}O$ from the enzyme, catalyzed by the following variants of HCA II: (◆) wild type, (△) Y7F, (○) N62L, and (■) N67L. Conditions were the same as in Figure 2. All of these data were observed at 25 °C.

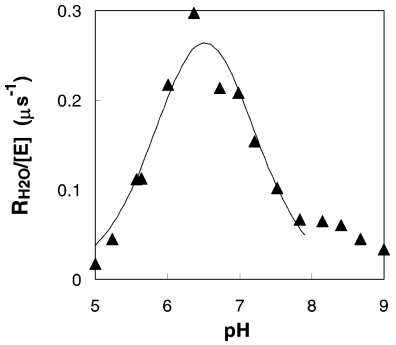

FIGURE 4: pH profile of R_{H_2O}/[E] in catalysis by Y7F and measured at 10 °C. Other conditions as listed in Figure 2.

For the N62L HCA II mutant crystallized at pH 8.2, the His64 side chain appears entirely in the inward position, with no evidence of the outward orientation (Figure 6A). The side chain of Leu62 has also shifted compared to that of Asn62 in the wild type (Figure 1). In this mutant, Leu62 moved into a more hydrophobic region in close proximity to Leu60. Because of the alternate conformation of Leu62 away from the solvated area in the active site, this side chain appears to have little influence upon disrupting the network of ordered water molecules. Consistent with this, the water network is conserved with that of the wild type but with the hydrogen bond between Leu62 and W3b removed (Figure 6A).

In contrast to the N62L HCA II at pH 8.2 structure, the N67L HCA II active-site water network is completely disrupted at the same pH (Figure 6B) and His64 is observed to be entirely in the outward position. The conformation of the side chain of Leu67 is consistent with that of Asn67 in

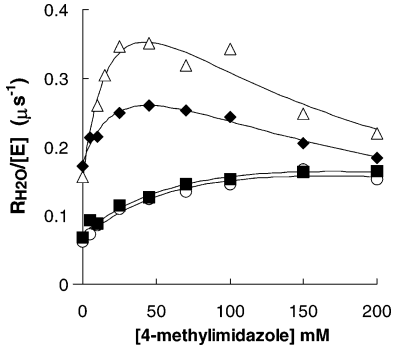

FIGURE 5: Enhancement by 4-MI of R_{H_2O}/[E] catalyzed by the following variants of HCA II: (◆) wild type, (△) Y7F, (○) N62L, and (■) N67L. Data were obtained at pH 7.8 with other conditions as described in Figure 2.

the wild type. The presence of this hydrophobic residue at position 67 most likely caused the observed disruption and consequent displacement of the waters in the active site (Figure 6B).

In the Y7F HCA II mutant structures at pH 8.2 and 10.0 (ammonium sulfate precipitant) and pH 9.0 (sodium citrate precipitant), the water network is mostly conserved (Figure 7). As might be expected, the loss of the hydroxyl group at residue 7 in Y7F HCA II resulted in the removal of water molecule W3a, which is part of the active-site water network in wild-type HCA II (Figure 1). The side chain of Phe7 occupied a similar orientation as Tyr7 in wild-type HCA II, with His64 entirely in the inward position with no observed dual conformation at this resolution (Figure 7C). When Y7F was crystallized using ammonium sulfate as the precipitant, a sulfate ion was observed bound to the zinc at pH 8.2 (Figure 7A). In wild-type HCA II, sulfate binding at the zinc only occurs at low pH (~5.0) as determined from both the crystal structure (*4*) and inhibition of catalysis (*27*). In the mutant Y7F HCA II, Phe7 could be causing a higher affinity of sulfate in the active site.

From structural studies of wild-type HCA II, it is known that the presence of sulfate does not affect the water network or the orientation of His64 in the active site (*4*). To assess the effect of sulfate in the N62L and N67L HCA II mutants, their structures were determined at pH 6.0 to induce sulfate binding. As predicted, sulfate was observed bound in both of these mutants and the conformation of His64 was unchanged (parts C and D of Figure 6). His64 was either all in the inward orientation for the N62L HCA II structure or all in the outward orientation for the N67L HCA II structure.

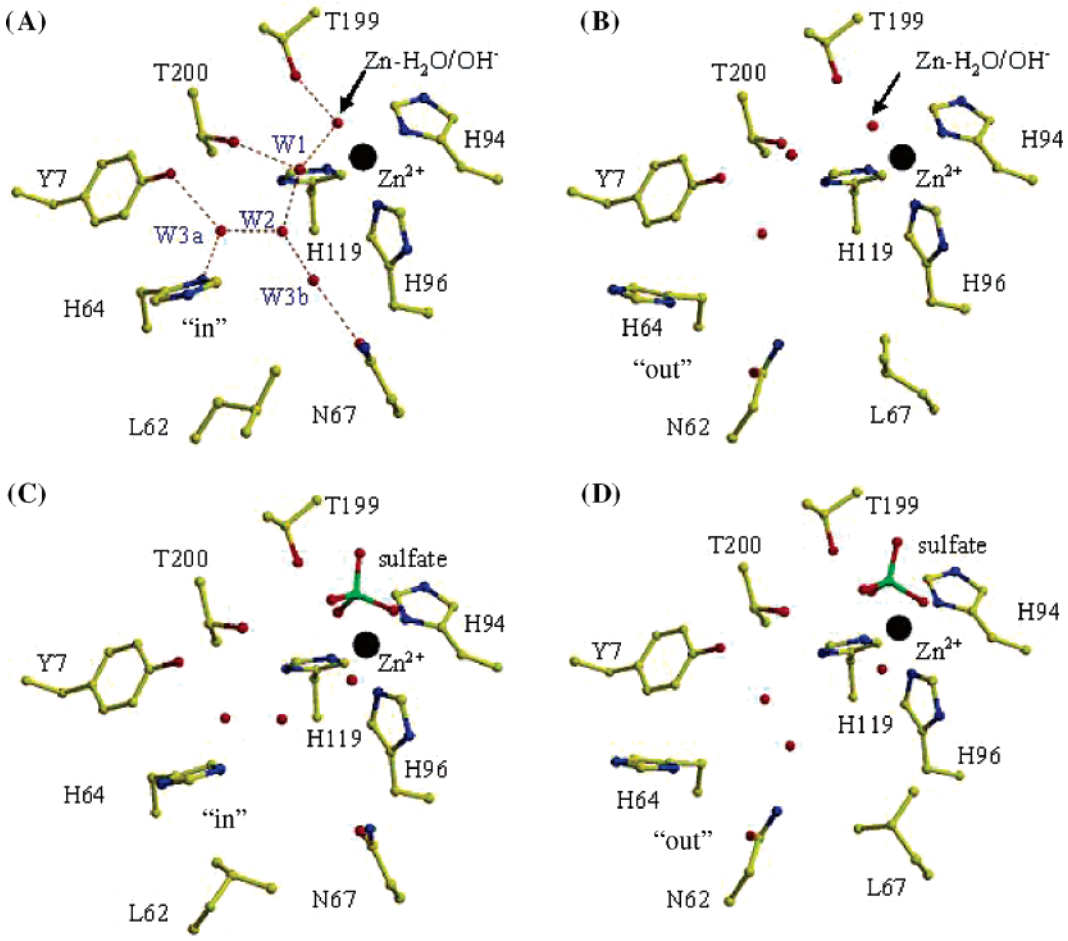

FIGURE 6: Active site of site-specific mutants of HCA II crystallized at pH 8.2 and 6.0. (A) N62L at pH 8.2, (B) N67L at pH 8.2, (C) N62L at pH 6.0, and (D) N67L at pH 6.0. Active-site residues are shown as yellow ball-and-stick models; the zinc atom is a black sphere; and solvent water molecules are red spheres. This figure was generated and rendered with BobScript and Raster3D, respectively (*39*, *40*).

Therefore, the determination of all three mutant structures in the presence and absence of sulfate indicates that sulfate binding does not have any significant effect on the crystal structures of either His64 conformation or the active-site water network (Figures 6 and 7).

An interesting observation was the effect of pH on the conformation of Leu62 in the N62L HCA II structures, which exhibits a pH-dependent preferred orientation (parts A and C of Figure 6). At the lower pH 6.0, Leu62 extends more into the active site and appears to disrupt the water network in a similar way to Leu67 in N67L HCA II (Figure 6B). This is in contrast to its conformation at pH 8.2, where it folds back into a hydrophobic region without affecting the solvent network (Figure 6A).

The Y7F HCA II mutant structure was determined at pH 10.0 in an attempt to have a sulfate-free active site. Unexpectedly, sulfate was still bound even at this high pH; however, the water network was still intact, and His64 still occupied the inward position exclusively. Because efforts to remove the zinc-bound sulfate by changing the pH of ammonium-sulfate-grown crystals were unsuccessful, crystals were prepared using sodium citrate as described in the Materials and Methods. These efforts resulted in the high-resolution structure of Y7F HCA II at pH 9.0 to 1.15 Å resolution, which lacked the zinc-bound sulfate. Additionally, there were no observable structural changes compared to the sulfate-containing crystal structures (Figures 6 and 7).

DISCUSSION

We have replaced three hydrophilic residues in the active-site cavity of HCA II with residues of approximately equivalent size but with hydrophobic characteristics (Y7F, N62L, and N67L HCA II). Each of these residues in wild-type HCA II are hydrogen-bonded to a conserved water in a network of ordered hydrogen-bonded waters observed in the X-ray crystal structure (Figure 1). We have determined that these substituted amino acids have effects on both structure and catalysis; they cause changes in the water structure in the active site, changes in the apparent pK_a, changes in ratios of inward and outward conformations of the side chain of the proton shuttle His64, and changes in the rate constant for proton transfer in catalysis between His64 and the zinc-bound water.

Catalysis. In general, the mutations at positions 7, 62, and 67 caused, at most, minor changes in the rate constants that report the catalytic interconversion of CO_2 and bicarbonate. Measurements by ^{18}O exchange of k_{cat}^{ex}/K_{eff}^{S} for the hydration of CO_2, the first stage of catalysis (eqs 1 and 3), showed no substantial changes between the wild type and mutants of HCA II of this study (Figure 2 and Table 3). The apparent p$K_{a\ ZnH_2O}$ obtained from the pH profile of k_{cat}^{ex}/K_{eff}^{S} represents the ionization of the zinc-bound water, and these values were also similar for the wild-type enzyme and mutants (Table 2). The values of the apparent p$K_{a\ ZnH_2O}$ were also

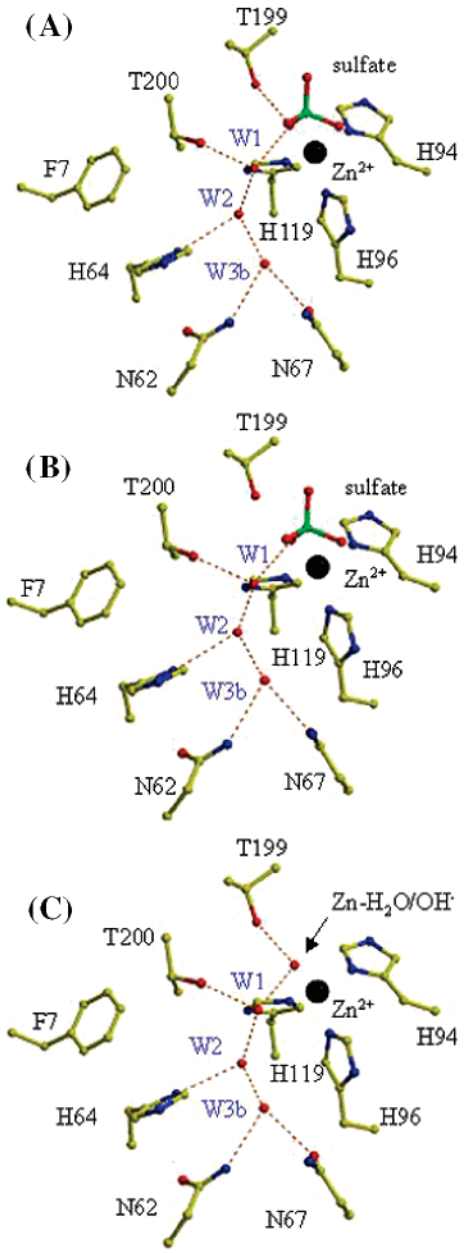

FIGURE 7: Active site of Y7F HCA II crystallized at various pH. (A) pH 8.2, (B) pH 10.0, and (C) pH 9.0 crystallized with sodium citrate. Active-site residues are shown as yellow ball-and-stick models; the zinc atom is a black sphere; and solvent water molecules are red spheres. This figure was generated and rendered with BobScript and Raster3D, respectively (*39*, *40*).

obtained from the catalyzed hydrolysis of 4-nitrophenylacetate, also given in Table 2. These data signify no large changes in the structure in the near vicinity of the zinc for the mutants compared with the wild type [confirmed by X-ray crystallography (Figures 6 and 7)] and no substantial changes in the chemistry of the catalysis of interconversion of CO_2 and bicarbonate. This is not unexpected because each of the side chains of residues 7, 62, and 67 are 7−9 Å from the active-site zinc. The residues that affect the hydration of CO_2 are closer to the metal, such as Thr199 and Glu106 (~4.0 Å for both) (*28*, *29*).

In the second stage of the catalysis (eqs 2 and 4), protons are transferred between His64 and the zinc-bound solvent (*1*, *7*). The mutants Y7F, N62L, and N67L HCA II all displayed evidence of altered proton transfer compared with the wild type, as evident in the pH profiles of R_{H_2O}/[E] (Figure 3), a rate constant for the release of $H_2{}^{18}O$ from the enzyme to solution, which depends upon proton transfer to the zinc-bound, ^{18}O-labeled hydroxide in the dehydration direction (eq 4). These data have been analyzed in terms of eq 6, which describes proton transfer from a donor group (predominantly His64) to the zinc-bound hydroxide, predicting a bell-shaped pH profile for R_{H_2O}/[E]. Such bell-shaped pH profiles were observed over the range of pH from 5 to 8 for wild-type, Y7F, and N67L HCA II (Figures 3 and 4); the values of R_{H_2O}/[E] for N62L HCA II were less dependent upon pH. Each of the pH profiles of Figures 3 and 4 showed a region of pH independence at pH > 8; we do not know the source of this effect, although it may represent the dissociation of ^{18}O-labeled hydroxide from the metal.

The interpretation of these bell-shaped curves requires accurate assignment of the pK_a values because switching the assignments of the pK_a for the donor and acceptor also fits the data (*30*). We have listed in Table 2 the values of $pK_{a\ ZnH_2O}$ for the zinc-bound water determined in two independent experiments: from pH profiles of k_{cat}^{ex}/K_{eff}^{S} for the hydration of CO_2 determined by ^{18}O exchange and of k_{cat}/K_m for the hydrolysis of 4-nitrophenylacetate. These confirm the assignment of $pK_{a\ ZnH_2O}$ used in fitting the data of Figures 3 and 4. The parameters of this fit to the bell-shaped components of Figure 3 (and Figure 4 for Y7F at 10 °C) are given in Tables 2 and 3, showing that the rate constant for proton-transfer k_B (eq 6) appears considerably larger for Y7F and lower for N67L HCA II compared with that for the wild type. In fact, the value of k_B for Y7F HCA II near 4 μs^{-1} at 10 °C (an estimated value is 7 μs^{-1} at 25 °C) is the largest observed for a carbonic anhydrase to our knowledge. This is explained in part by the more acidic pK_a of His64 in Y7F compared with that in the wild type (Table 2) and in part to structural effects discussed below.

Maximal values of the steady-state constant k_{cat} for hydration catalyzed by Y7F HCA II were determined by Liang et al. (*28*) to be similar to those for the wild type, also consistent with the results of Table 3. For dehydration, values of k_{cat} are smaller for Y7F HCA II compared with that for the wild type (Table 3). However, these data are not inconsistent with the ^{18}O-exchange results on k_B discussed above. The value of k_{cat} depends upon several steps in the catalysis, whereas k_B obtained from ^{18}O-exchange experiments is more representative of intramolecular proton transfer and less dependent upon other steps of the catalysis. The SHIEs are helpful in this regard. The SHIE on the maximal value of k_B was 2.5 observed for catalysis by Y7F HCA II in the dehydration direction and consistent with a rate-limiting proton transfer. The maximal value of k_B in H_2O was 4 μs^{-1}. The SHIE on k_{cat} for dehydration catalyzed by Y7F was slightly inverse at 0.81 ± 0.10 on a value of k_{cat} in H_2O of 0.05 μs^{-1}, strongly suggesting that steps other than proton transfer are rate-limiting, perhaps the dissociation of product bicarbonate from the enzyme. It is interesting that the SHIE on k_{cat}/K_m for dehydration catalyzed by Y7F was also inverse at 0.74 ± 0.07. This is not unprecedented with the carbonic anhydrases; inverse isotope effects are commonly observed on the esterase function (*8*, *31*).

In addition, the difference between k_{cat} at steady state and k_B at chemical equilibrium (Table 3) reflects the different natures of these experiments. The steady-state experiment in the dehydration direction reflects the necessity of a net proton flux from His64 to the zinc-bound hydroxide. The steady-state concentration of protonated His64 at maximum velocity is expected to be greater than the equilibrium concentration because it represents a species accumulating before a rate-limiting step. The ^{18}O experiment involves equilibrium concentrations of enzyme species and does not involve a net flux of protons.

The steady-state experiment requires the presence of buffers, and there is evidence that catalysis by Y7F HCA II is more susceptible to a contribution of buffer to proton transfer than the other enzymes of Table 3. The enhancement of catalysis by Y7F HCA II caused by the addition of 4-MI (Figure 5) may be due as much to electrostatics and solvation in the active-site cavity as with removing steric contrictions; i.e., the Phe7 side chain of Y7F overlaps that of Tyr 7 in the crystal structures (Figures 5 and 6). Other kinetic data are consistent with an enhanced access into the active site of Y7F; for example, the catalyzed esterase hydrolysis is appreciably greater for Y7F than for wild-type HCA II or the other mutants (Table 3 and Supplementary Figure 2 in the Supporting Information).

Structure. The side-chain orientation of His64 in wild-type HCA II has been observed by X-ray crystallographic studies to have two orientations that appear about equally occupied near physiological pH, one inward with the side chain oriented toward the zinc at the active site and a second outward with the side chain oriented toward and in partial contact with bulk solution (*3*, *4*). The mutants Y7F and N62L both have nearly a total fraction of His64 in an inward conformation (Figures 6 and 7) (*3*, *4*). N67L has an outward conformation (Figure 6).

Computations suggest that the efficiency of intramolecular proton transfer in HCA II is strongly dependent upon the solvation structure in the active site and particularly the number of water molecules through which this transfer proceeds (*32*, *33*). It is hypothesized that a significant limit in the rate of proton shuttling in carbonic anhydrase would be the capture of a proton in the form of a solvent species with partial hydronium ion character H_3O^+ in an Eigen-like complex ($H_9O_4^+$) during the catalysis (*32*, *34*, *35*). Specifically, the solvent molecule W2 could have such character because it appears hydrogen-bonded with three adjacent solvent molecules (W1, W3a, and W3b) in a semi-pyramidal arrangement (*3*, *4*) resembling the solvated hydronium ion in such an Eigen ion complex (*36*). In fact, computations show a much more efficient proton transfer without a branched solvent structure, allowing for a more concerted proton transfer without passing through a partial hydronium ion (*32*). We can evaluate this hypothesis with the mutant Tyr7, in which the solvent molecule W3a is not observed in the crystal structure. This structure, if applicable to the proton transfer, would prevent the formation of the stable and possible rate-limiting $H_9O_4^+$ in the transition state.

The crystal structure of Y7F HCA II to 1.15 Å resolution showed that the W3a solvent molecule was indeed no longer observed in the array of ordered solvent molecules, and because the amino acid mutation was of similar volume to the wild type, there was no further disruption of the remaining solvent network compared with the wild type (Figure 7). Furthermore, the Y7F mutation caused His64 to be in an inward-only conformation and directly hydrogen-bonded with W2, whereas in the wild type, His64 showed weak electrostatic interactions (~3.4 Å) with W2, W3a, and W3b.

We suggest that the very efficient proton transfer observed for Y7F HCA II may be due to the combined effect of the following three features of the structure that we have observed. First, in this mutant, the side chain of His64 showed an appreciable orientation pointing toward the active-site zinc. We believe that access to an inward conformation is necessary but not sufficient for efficient proton transfer. An et al. (*11*) presented arguments to show that His64 in the outward conformation considered alone is not associated with proton transfer in catalysis. However, a suggestion that the orientation of His64 found in the crystal structures may not reflect its efficiency in proton transfer was made after observing that the mutation T200S caused a change in the orientation of His64 with little consequence to the catalysis compared with the wild type (*37*).

Second, in the structure of Y7F, there is observed an array of single water molecules, not branched, between the proton donor His64 and acceptor zinc-bound hydroxide. Although the relationship between the water structure observed in the crystal and that necessary for proton transfer is problematic, the crystal structure shows an ordered solvent network that may represent fragments of a dynamic water structure that provides a proton-transfer pathway. The observation of a nonbranched water structure in the crystal should indicate that such a structure is represented among the ensemble of flickering arrays of active-site water, structures with lifetimes measured in picoseconds. It is this expectation that links these results with the computations of proton transfer and solution studies. Third is the acidic pK_a of His64 in Y7F HCA II, making this side chain a better proton donor in the dehydration direction (Table 3).

This combination of features supporting rapid proton transfer was not observed for N67L and N62L HCA II, which show values of k_B at 0.2 and 0.1 μs^{-1} (Table 3). N67L has an outward orientation of His64 with an ordered water structure much decreased compared with wild-type and Y7F HCA II (Figures 6 and 7). The data for N62L HCA II were difficult to interpret because it had a complex pH dependence (Figure 3). Its structure shows His64 in the inward orientation but is observed to have a pH-dependent conformation of the side chain of Leu62 that probably complicates the kinetics of its catalysis (Figure 6).

Although the effect of the mutations of residues 7, 62, and 67 is complex on the structure and catalysis, the data do lend a significant overall conclusion. These residues appear to fine-tune the proton-transfer efficiency of His64, while having a much smaller effect on the interconversion of CO_2 and bicarbonate. It is significant that the identity of these residues (Tyr7, Asn62, and Asn67) is invariant in CA II from a wide range of species from chicken, rodents, bovine, and humans (*38*). Moreover, these residues are not conserved in isozymes of carbonic anhydrase in the α class that do not have histidine at residue 64, such as HCA III with Lys64 and Arg67. In addition, CA II has the advantage, with the pK_a of both His64 and the zinc-bound solvent near 7, to have maximal velocity about equal in the hydration

and dehydration directions, a necessary feature because catalysis in both directions is utilized in the physiological function of carbonic anhydrase. With a mutant such as Y7F, the ΔpK_a near 1.0 between the acceptor and donor ($pK_{a\ ZnH_2O} - pK_{a\ His64}$) is more favorable for proton transfer in the dehydration direction according to free-energy plots (*11*) but may be less favorable at −1.0 in the hydration direction. These are features of the fine-tuning of the active site with respect to proton transfer.

ACKNOWLEDGMENT

The authors would like to thank the staff at the SER-CAT 22-ID beamline at APS, Argonne National Laboratory for assistance during X-ray diffraction data collection.

SUPPORTING INFORMATION AVAILABLE

pH profiles of k_{cat} (s^{-1}) for catalysis by Y7F, N62L, and, N67L HCA II (Supplementary Figure 1) and pH dependence of k_{cat}/K_m ($mM^{-1}\ s^{-1}$) for the hydrolysis of 4-nitrophenylacetate by Y7F, N62L, and N67L HCA II (Supplementary Figure 2). This material is available free of charge via the Internet at http://pubs.acs.org.

REFERENCES

1. Tu, C. K., Silverman, D. N., Forsman, C., Jonsson, B. H., and Lindskog, S. (1989) Role of histidine 64 in the catalytic mechanism of human carbonic anhydrase II studied with a site-specific mutant, *Biochemistry 28*, 7913−7918.
2. Jude, K. M., Wright, S. K., Tu, C., Silverman, D. N., Viola, R. E., and Christianson, D. W. (2002) Crystal structure of F65A/Y131C-methylimidazole carbonic anhydrase V reveals architectural features of an engineered proton shuttle, *Biochemistry 41*, 2485−2491.
3. Nair, S. K., and Christianson, D. W. (1991) Unexpected pH-dependent conformation of His-64, the proton shuttle of carbonic anhydrase II, *J. Am. Chem. Soc. 113*, 9455−9458.
4. Fisher, Z., Prada, J. A. H., Tu, C., Duda, D., Yoshioka, C., An, H. Q., Govindasamy, L., Silverman, D. N., and McKenna, R. (2005) Structural and kinetic characterization of active-site histidine as a proton shuttle in catalysis by human carbonic anhydrase II, *Biochemistry 44*, 1097−1105.
5. Christianson, D. W., and Fierke, C. A. (1996) Carbonic anhydrase: Evolution of the zinc binding site by nature and by design, *Acc. Chem. Res. 29*, 331−339.
6. Silverman, D. N., and Lindskog, S. (1988) The catalytic mechanism of carbonic anhydrase−Implications of a rate-limiting protolysis of water, *Acc. Chem. Res. 21*, 30−36.
7. Lindskog, S. (1997) Structure and mechanism of carbonic anhydrase, *Pharmacol. Ther. 74*, 1−20.
8. Steiner, H., Jonsson, B. H., and Lindskog, S. (1975) Catalytic mechanism of carbonic anhydrase−Hydrogen isotope effects on kinetic parameters of human C isoenzyme, *Eur. J. Biochem. 59*, 253−259.
9. Duda, D., Tu, C. K., Qian, M. Z., Laipis, P., Agbandje-McKenna, M., Silverman, D. N., and McKenna, R. (2001) Structural and kinetic analysis of the chemical rescue of the proton transfer function of carbonic anhydrase II, *Biochemistry 40*, 1741−1748.
10. Jackman, J. E., Merz, K. M., Jr., and Fierke, C. A. (1996) Disruption of the active site solvent network in carbonic anhydrase II decreases the efficiency of proton transfer, *Biochemistry 35*, 16421−16428.
11. An, H., Tu, C., Duda, D., Montanez-Clemente, I., Math, K., Laipis, P. J., McKenna, R., and Silverman, D. N. (2002) Chemical rescue in catalysis by human carbonic anhydrases II and III, *Biochemistry 41*, 3235−3242.
12. Khalifah, R. G., Strader, D. J., Bryant, S. H., and Gibson, S. M. (1977) ^{13}C nuclear magnetic resonance probe of active-site ionizations in human carbonic anhydrase B, *Biochemistry 16*, 2241−2247.
13. Segel, I. H. (1975) *Enzyme Kinetics*, Wiley-Interscience, New York.
14. Silverman, D. N. (1982) Carbonic anhydrase: Oxygen-18 exchange catalyzed by an enzyme with rate-contributing proton-transfer steps, *Methods Enzymol. 87*, 732−752.
15. Simonsson, I., Jonsson, B. H., and Lindskog, S. (1979) ^{13}C NMR study of CO_2 HCO_3 exchange catalyzed by human carbonic anhydrase C at chemical equilibrium, *Eur. J. Biochem. 93*, 409−417.
16. Khalifah, R. G. (1971) Carbon dioxide hydration activity of carbonic anhydrase. 1. Stop-flow kinetic studies on native human isoenzyme B and isoenzyme C, *J. Biol. Chem. 246*, 2561−2573.
17. Verpoorte, J. A., Mehta, S., and Edsall, J. T. (1967) Esterase activities of human carbonic anhydrases B and C, *J. Biol. Chem. 242*, 4221−4229.
18. Bell, R. P. (1973) *The Proton in Chemistry*, Cornell University Press, Ithaca, NY.
19. McPherson, A. (1982) *Preparation and Analysis of Protein Crystals*, Wiley, New York.
20. Otwinowski, Z., and Minor, W. (1997) Processing of X-ray diffraction data collected in oscillation mode, *Methods Enzymol. 276*, 307−326.
21. Emsley, P., and Cowtan, K. (2004) Coot: Model-building tools for molecular graphics, *Acta Crystallogr., Sect. D: Biol. Crystallogr. 60*, 2126−2132.
22. Brunger, A. T., Adams, P. D., Clore, G. M., DeLano, W. L., Gros, P., Grosse-Kunstleve, R. W., Jiang, J. S., Kuszewski, J., Nilges, M., Pannu, N. S., Read, R. J., Rice, L. M., Simonson, T., and Warren, G. L. (1998) Crystallography and NMR system: A new software suite for macromolecular structure determination, *Acta Crystallogr., Sect. D: Biol. Crystallogr. 54*, 905−921.
23. Sheldrick, G. M. (1997) Macromolecular crystallography, part B, *Methods Enzymol. 277*, 319−343.
24. Engh, R. A., and Huber, R. (1991) Accurate bond and angle parameters for X-ray protein-structure refinement, *Acta Crystallogr., Sect. A: Found. Crystallogr. 47*, 392−400.
25. Silverman, D. N., Tu, C., Chen, X., Tanhauser, S. M., Kresge, A. J., and Laipis, P. J. (1993) Rate−equilibria relationships in intramolecular proton transfer in human carbonic anhydrase III, *Biochemistry 32*, 10757−10762.
26. Elder, I., Tu, C. K., Ming, L. J., McKenna, R., and Silverman, D. N. (2005) Proton transfer from exogenous donors in catalysis by human carbonic anhydrase II, *Arch. Biochem. Biophys. 437*, 106−114.
27. Simonsson, I., and Lindskog, S. (1982) The interaction of sulfate with carbonic-anhydrase, *Eur. J. Biochem. 123*, 29−36.
28. Liang, Z. W., Xue, Y. F., Behravan, G., Jonsson, B. H., and Lindskog, S. (1993) Importance of the conserved active-site residues Tyr7, Glu106 and Thr199 for the catalytic function of human carbonic anhydrase II, *Eur. J. Biochem. 211*, 821−827.
29. Krebs, J. F., Ippolito, J. A., Christianson, D. W., and Fierke, C. A. (1993) Structural and functional importance of a conserved hydrogen-bond network in human carbonic anhydrase II, *J. Biol. Chem. 268*, 27458−27466.
30. Tipton, K. F., and Dixon, H. B. F. (1979) Effects of pH on enzymes, *Methods Enzymol. 63*, 183−234.
31. Pocker, Y., and Bjorkquist, D. W. (1977) Comparative studies of bovine carbonic anhydrase in H_2O and D_2O. Stopped-flow studies of the kinetics of interconversion of CO_2 and HCO_3, *Biochemistry 16*, 5698−5707.
32. Cui, Q., and Karplus, M. (2003) Is a "proton wire" concerted or stepwise? A model study of proton transfer in carbonic anhydrase, *J. Phys. Chem. B 107*, 1071−1078.
33. Lu, D. S., and Voth, G. A. (1998) Proton transfer in the enzyme carbonic anhydrase: An ab initio study, *J. Am. Chem. Soc. 120*, 4006−4014.
34. Wu, Y., and Voth, G. A. (2003) A computer simulation study of the hydrated proton in a synthetic proton channel, *Biophys. J. 85*, 864−875.
35. Brewer, M. L., Schmitt, U. W., and Voth, G. A. (2001) The formation and dynamics of proton wires in channel environments, *Biophys. J. 80*, 1691−1702.
36. Eigen, M. (1964) Proton transfer acid−base catalysis and enzymatic hydrolysis. I. Elementary processes, *Angew. Chem., Int. Ed. 3*, 1−19.

37. Krebs, J. F., Fierke, C. A., Alexander, R. S., and Christianson, D. W. (1991) Conformational mobility of His-64 in the Thr-200 to Ser mutant of human carbonic anhydrase II, *Biochemistry 30*, 9153−9160.
38. HewettEmmett, D., and Tashian, R. E. (1996) Functional diversity, conservation, and convergence in the evolution of the α-, *β*-, and *γ*-carbonic anhydrase gene families, *Mol. Phylogenet. Evol. 5*, 50−77.
39. Merritt, E. A., and Bacon, D. J. (1997) Raster3D version 2: Photorealistic molecular graphics, *Methods Enzymol. 277*, 505−524.
40. Esnouf, R. M. (1997) An extensively modified version of MolScript that includes greatly enhanced coloring capabilities, *J. Mol. Graphics Modell. 15*, 112−113, 132−134.

BI602620K